Predicting the anchoring of liquid crystals at a solid surface: 5-cyanobiphenyl on cristobalite and glassy silica surfaces of increasing roughness

Otello Maria Roscioni, Luca Muccioli,* Raffaele Guido Della Valle, Antonio Pizzirusso, Matteo Ricci, and Claudio Zannoni*

Dipartimento di Chimica Industriale "Toso Montanari" and INSTM, Università di Bologna, viale Risorgimento 4, IT-40136 Bologna, Italy

E-mail: luca.muccioli@unibo.it; claudio.zannoni@unibo.it

Rev. March 26, 2013

Abstract

We employ atomistic molecular dynamics simulations to predict alignment and anchoring strength of a typical nematic liquid crystal, 4-*n*-pentyl-4'-cyano biphenyl (5CB), on different forms of silica. In particular, we study a thin ($\sim$ 20 nm) film of 5CB supported on surfaces of crystalline (cristobalite) and amorphous silica of different roughness. We find that the orientational order at the surface and the anchoring strength depend on the morphology of the silica surface and its roughness. Cristobalite yields a uniform planar orientation and increases order at the surface with respect to bulk, while amorphous glass has a disordering effect. Despite the low order at the amorphous surfaces, a planar orientation is established with a persistence length into the film higher than the one obtained for cristobalite.

*To whom correspondence should be addressed

Introduction

The molecular organization of liquid crystals (LC) and other organic functional materials at their interface with a solid is of key importance for understanding and optimizing a variety of devices ranging from displays[1,2] to organic field effect transistors and organic solar cells,[3,4] just to cite a few. Given its importance, a large body of empirical knowledge has been collected about adhesion, *i.e.* the strength of interaction with the surface (as for ordinary liquids)[5–7] , but also for the orientation of LC molecules,[1,8–14] a property referred to as *anchoring*. The anchoring can be parallel to the surface with LC molecules arranged along a certain direction (homogeneous) or distributed isotropically on the surface (random planar), perpendicular (also called homeotropic) or tilted at a certain angle. The anisotropic anchoring strength w_2^A is commonly described by the so-called Rapini-Papoular (RP) expression:[15,16]

$$W(\beta) = w_0^A - \frac{1}{2} w_2^A \sin^2(\beta - \beta_{eq}) \tag{1}$$

which gives the surface free energy per unit area $W(\beta)$ required for changing the local preferred orientation (the director) from its equilibrium value, β_{eq}, here measured from the surface normal to β. The RP expression is useful to concisely summarize the behavior of nematics close to a surface and has been generalized to a more complete orthogonal expansion,[17] or to include an additional dependence on an azimuthal angle to express preference for an in-plane direction.[18]

A realistic theoretical or computational treatment that can predict the anchoring is however conspicuously lacking. This is particularly unpleasant as the observed empirical behavior can simultaneously depend on several features. For a given LC material, a fundamental one is of course the chemical nature of the substrate and its state: crystalline (and in that case the specific polymorph and the exposed facet) or glassy (with a certain preparation protocol and at a given distance from the glass transition temperature of the

material). Another important factor, inevitably present in any real substrate, is a certain amount of roughness, or more generally of structural defects making the support surface deviating from ideal flatness.

In a recent work[19] we have investigated this problem with atomistic molecular dynamics (MD) simulations, studying in detail the molecular organization and anchoring of thin films ($\sim$ 10 and 20 nm thick) of 4-*n*-pentyl-4'-cyano biphenyl (5CB) on an atomically flat (001) face of hydrogen-terminated crystalline silicon. We have determined for the first time, from the molecular level up, quantities like anchoring orientation and strength until now treated as purely empirical parameters. In the specific case of 5CB on Si:H, a strong homogeneous alignment of the 5CB molecules parallel to the surface was found as well as a homeotropic alignment at the vacuum exposed surface.[19]

No simulation results, as far as we are aware, are instead available for the important case of the anchoring of 5CB on silica (SiO_2) substrates and, more specifically, for amorphous glassy surfaces which, on the other hand, have been much studied experimentally,[10,14] together with silicon oxide SiO_x.[20–23] In particular, it has been shown in classical works by Janning[20] and others[21,22] that surfaces obtained from oblique evaporation of silicon oxide can induce planar, tilted, or bistable states of a nematic film in contact, depending on the parameters of the evaporation (angle, oxide thickness, evaporation rate). We should stress that the surface structures obtained with this procedure are very irregular[22] with corrugations and features like deposited silica columns of micrometric size, thus in a range of surface inhomogeneities where the alignment effects produced should be due to elastic distortions of the nematic director[12,18,24] rather than rather than the chemical nature or the roughness of the support as discussed here. The alignment of 5CB on more flat silica surfaces has also been studied, in particular on fused silica. There, a tilt angle was observed by Shen and co-workers using second harmonic generation (SHG)[10] on thin silica films prepared by oxidizing a silane derivative in a Ar/O_2 plasma[25] while on large angle electron beam evaporated SiO_2, a planar alignment

was found by Chen et al.[26] Some disagreement has also appeared in the literature on the interpretation of birefringence and SHG experiments leading to conclude on nearly homeotropic[27,28] or parallel[29] alignment of the first monolayer of 5CB on fused silica which is anyway planar in the bulk. Here we wish to study, using atomistic computer simulations, the alignment of 5CB on flat silica substrates and the effect of roughness on the nanoscale alignment. We shall discuss in particular the changes of ordering of the film detected on the surface, when going from a crystalline to an amorphous surface with a controlled roughness, and the role of electrostatic interactions between the silica support and the LC phase.

The paper is organized as follows. In the next section we describe the computational approach used to prepare first a crystalline cristobalite slab and then two silica glass slabs with a controlled root mean square (RMS) roughness. In the following sections we report a characterization of the electrostatic landscape close to the substrate and the results of the MD investigation for an isotropic and nematic state. A discussion section analyses these findings and summarizes the work.

Sample Preparation

Cristobalite

Cristobalite, one of the various forms of quartz, has a cubic $P2_13$ structure with experimental lattice parameter $a = 7.16$ Å.[30] Here the crystal structure was optimized at the molecular mechanics level of theory with the computer program GULP.[31,32] The pairwise interactions between silica and oxygen atoms were described with a potential of the form $V_{ij} = q_i q_j / r + A_{ij} exp(-B_{ij} r) - C_{ij} / r^6$, which consists of Coulomb and Buckingham terms. The charges and parameters for this potential were taken from reference 33. The optimized (0 K) lattice parameter $a = 7.06$ Å is in good agreement with the experimental structure.[30] From the optimized bulk structure we generated a 9x9 slab supercell with

a non-polar crystal termination, that exposes the (001) surface, with surface dimension 63.5Å$\times$63.5 Åand a thickness of about 60Å. It has been argued[34] that the effective support slab thickness interacting with a liquid crystal is not just the superficial layer but a three dimensional region of thickness up to 14 Å (at least for muscovite mica). Thus our slab of 60 Å is sufficiently thick to avoid finite size effects of the support. The positions of atoms on the exposed crystal surface were relaxed with a geometrical minimization at 0K in order to obtain a dipole-free minimum energy structure.

Amorphous Silica

A bulk sample of an amorphous silica glass was prepared according to the procedure described in reference 35. Briefly, a orthorhombic box was created by replicating the unit crystal cell of cristobalite. The resulting super-cell lattice vectors were adjusted to achieve the experimentally determined density of vitreous silica at room temperature (2.2 g/cm^3) and kept fixed in order to avoid formation of 6-fold coordinated silicon atoms.[35] MD simulations of a sample of 4608 SiO_2 units (13824 atoms) were then carried out in the NVT ensemble with the program LAMMPS.[36,37] The sample was heated to 4000 K to obtain liquid silica and then cooled (10 K/ps) to 300 K to give an amorphous silica glass. The pairwise interactions between silica and oxygen atoms were the same used for cristobalite.[33] With these settings, we obtained a sample of amorphous silica whose properties, and in particular the radial distribution functions $g_{Si-Si}(r)$, $g_{O-O}(r)$, $g_{Si-O}(r)$ are in good agreement with previous studies[33,35] and experimental data.[38]

Two free surfaces were then obtained by removing the periodic boundary conditions of the simulation box in one direction, giving a model slab with surface dimensions 58.7 $\times$ 58.7 Å and a thickness of about 60 Å. Random defects were created by removing SiO_2 units from the surface layers of the resulting slabs, in order to increase the roughness of the otherwise atomically flat surfaces. To help the local surface reconstruction after this surgery, a thermal annealing at 900 K was carried out for 1 ns, after which the system was

cooled to 300 K at a rate of 5 K/ps. The sample energies were finally minimized at 0 K to yield the structures employed in the following MD simulations. It is worth mentioning that thanks to the non covalent pair potential chosen, atoms can move on the surface and find new optimized positions.

As the two surfaces have identical dimensions and composition, the only difference between them is due to their surface topography. The morphology of the amorphous silica surfaces depends on the number of SiO_2 units removed in each slab, and on the reconstruction which the surface undergoes after the simulated thermal annealing. The roughness of each surface was computed as the the root mean square (RMS) deviation, σ_R, of its solvent-accessible surface (SAS) along the direction normal to the surface. The SAS was computed using the rolling-sphere algorithm, as implemented in the program 3V:[39,40] A spherical probe with radius 1.6 Å was used in the calculations, while silicon and oxygen atoms were represented as hard spheres with radii of 2.10 and 1.52 Å, respectively (values taken from the Open Babel library[41–44]). We found that the first sample (nicknamed *smooth*) has a RMS of 1.5 Å, while the second sample (*rough*) has a RMS of 3.2 Å. As a reference, the cristobalite (001) surface has a roughness of 0.7 Å: since the surface roughness of cristobalite (001) is lower than the Si, O atomic radii, we can say it is atomically flat. We notice that the RMS of these surfaces, although seemingly small, is rather common in modern technology, e.g. it is similar to those of modern magnetic hard disk glass substrates.[45]

5CB on silica

The LC films studied in this work consisted of 2000 molecules of 5CB laying on top of the three silica surfaces just described, namely the cristobalite (001) surface and the two surfaces of amorphous silica with different roughness.

The molecules of 5CB were modelled with a united-atom force field developed and validated by Tiberio *et al.*[46] The 5CB–SiO_2 interaction was described through a set of

pairwise terms, each formed by a long-range Coulomb part plus a shorter-range Lennard-Jones part, *i.e.* $V_{ij} = q_i q_j / r + \epsilon_{ij}[(R_{min,ij}/r)^{12} - 2(R_{min,ij}/r)^6]$. The usual Lorentz-Berthelot mixing rules[47] were applied, with the parameters for Si and O atoms taken from the work of Cruz-Chu *et al.*[48] and reported here in Table 1 for convenience. These parameters were chosen because they reproduce the wettability of real silica surfaces without explicitly including surface OH groups.[48] In this way we obtained silica surfaces whose properties are similar to those of commonly used glass substrates.

The MD simulations were carried out with the program NAMD[49] in the NVT ensemble at T = 300 K and T = 320 K for the nematic and isotropic phases of the 5CB, respectively. In the simulated samples, the silicon and oxygen atoms belonging to the silica slab were kept frozen to their equilibrium position, as recommended in reference.[48] MD trajectories were followed for a minimum of 90 ns up to 160 ns including equilibration, with the following time windows for the production runs of the different systems: cristobalite: 53 ns at 300 K and 90 ns at 320 K; smooth amorphous silica: 76 ns at 300 K, 46 ns at 320 K; rough amorphous silica: 70 ns at 300 K; 80 ns at 320 K.

Table 1: Force field parameters for the Lennard-Jones term, taken from ref.[48]

species	ϵ (kcal/mol)	r_{min} (Å)	q (e)
Si	0.30	3.500	0.90
O	0.15	4.295	−0.45

A side view of the three silica slabs and of the LC sample placed on top of each is shown in Figure 1. The difference in roughness between the surfaces, which is detectable from the snapshots, is defined in a quantitative way by the SASs shown in the bottom plates of Figure 2.

Electrostatic Potential Energy Landscapes

As a consequence of the force field chosen, the longest-range interaction between the silica surface and the 5CB phase is essentially electrostatic. It is interesting to see to what

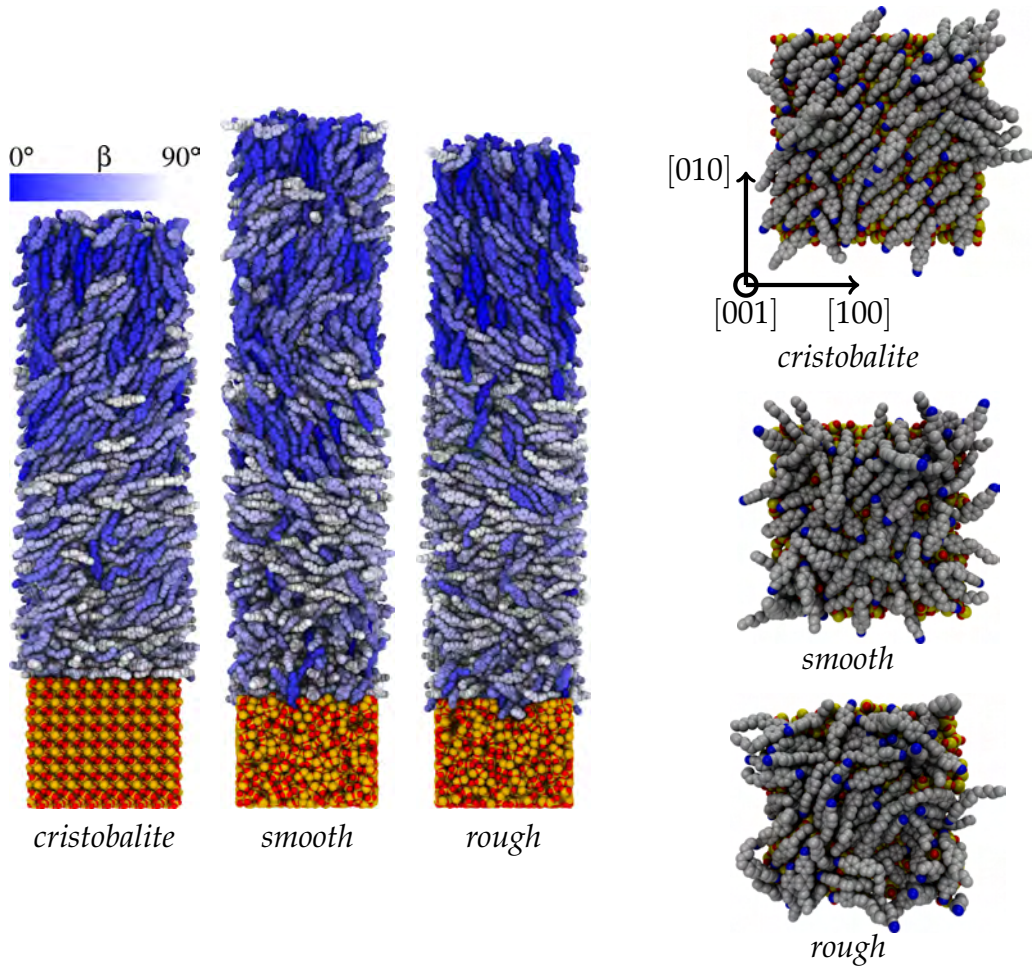

Figure 1: Lateral view (left panel) of the samples of 2000 5CB molecules supported on each silica surface and close-up view (right panel) of a typical snapshot of the overlayer at each support/LC interface at T = 300 K. The 5CB molecules director of this first layer is aligned preferentially along the [110] direction over the cristobalite (001) surface, while the other two show no in plane preference. Molecules are color coded according to their orientation with respect to the surface, ranging from blue (perpendicular) to grey (parallel).

extent it propagates away from the surface and if its range depends on surface morphologies. The electrostatic potential (EP) energy for a 2-dimensional slab was computed summing over partial atomic charges using an approach analogous to that of the Ewald sum, developed by Parry[50,51] and implemented in the computer program GULP.[31,32] We recall that the Parry summation method is the most accurate technique for calculations of long-range Coulomb energy for systems with slab geometry.[52] However, the classic 3D particle-mesh Ewald summation method (coupled with a large vacuum gap) was used

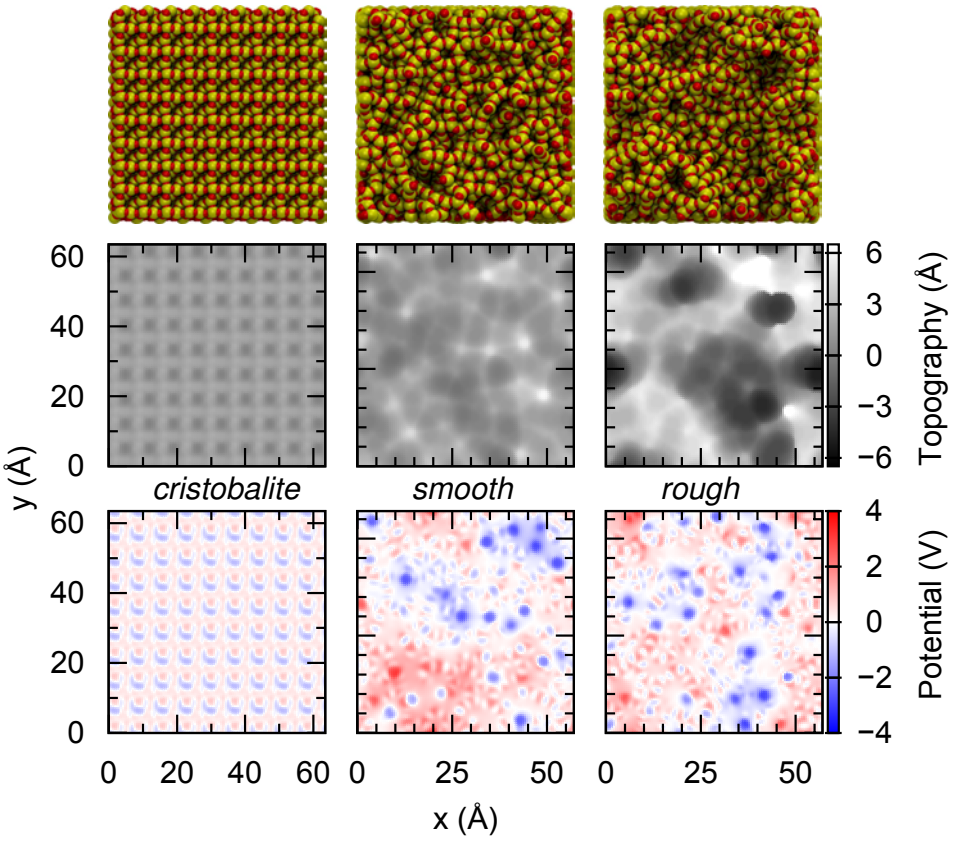

Figure 2: Top view of cristobalite (001) (RMS roughness σ_R = 0.7 Å, top-left panel), *smooth* amorphous surface (σ_R= 1.5 Å, top-center panel) and *rough* amorphous surface (σ_R = 3.2 Å, top-right panel). The corresponding surface topography is shown as the solvent accessible surface (middle panels) and the colour-coded electrostatic potential maps computed on the SAS is shown in the bottom panels. Oxygen atoms are shown in red, silicon atoms in yellow.

in subsequent MD simulations with NAMD as it is computationally much more efficient. The atoms constituting the slab were assigned point charges with a value of 0.90 e and −0.45 e for silicon and oxygen atoms, respectively.[48]

EP landscapes above silica surfaces were obtained by computing the electrostatic energy of a positive test charge of +1 e over a grid of points representing the SAS. The resulting multi-dimensional maps are shown in the bottom plates of Figure 2. As expected for neutral, dipole-less slabs, the mean value of the EP averaged above each surface is zero.[53] For the cristobalite (001) surface, a dense pattern of positive and negative regions occurs regularly on the surface, reflecting the periodic structure of the underlying crystal

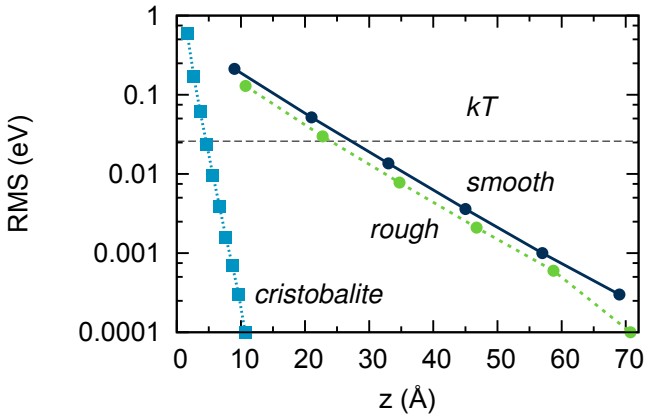

Figure 3: RMS value of the electrostatic potential energy above the silica support. Dotted, solid and dashed lines refer to cristobalite (001), *smooth* and *rough* surfaces, respectively. The horizontal line shows the value of kT at 300 K.

facet. For the two amorphous silica surfaces, the EP is partitioned into irregular regions with values ranging from -3 to +3 V (Figure 2). Furthermore, no evident correlation was found between the silica surface morphology and the value of EP.

Even if the mean value of the EP on each plane is zero, it is interesting to study its fluctuations and more specifically the RMS value measuring the intensity of the oscillations between positive and negative regions. To study the behavior of the EP above each surface, we computed the RMS EP for planes at progressively increasing distances from the silica surface. When the RMS value becomes of the same order of thermal fluctuations ($\sim k$T), it is safe to assume that the surface has no longer a direct influence on the substrate. For the amorphous surfaces we have found that RMS fluctuations decay exponentially as a function of the distance, as shown in Figure 3, and that they are of the same order of kT at 300 K at a distance of about 2.5 nm. As a consequence we might expect the 5CB alignment to be directly perturbed electrostatically by the support at least up to this distance. The RMS fluctuations computed above the cristobalite surface revealed that the EP at the surface (z=0) has a strength comparable to that of the amorphous samples, while it decays much more rapidly and it drops below kT at 300 K at just 5 Å.

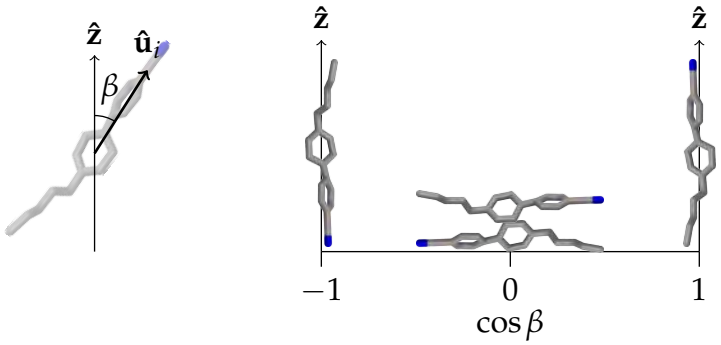

Figure 4: Definition of the orientation of a 5CB molecule with respect to the axis normal to the surface. The tilt angle β is defined as the angle between the molecule fixed unit vector $\hat{\mathbf{u}}$ and the normal at the surface, $\hat{\mathbf{z}}$.

Results

Molecular Organization of 5CB Films

We define the molecular orientation of each 5CB molecule in terms of the angle between the molecular axis $\hat{\mathbf{u}}$, chosen as the principal axis of inertia, and the normal to the surface, $\hat{\mathbf{z}}$. With this notation, a molecule will have a $\cos\beta = -1$, 1, 0 when the CN group of a molecule of 5CB is pointing towards, away from or parallel to the silica surface, as shown in Figure 4. To study the molecular organization of 5CB across the film, we have computed the one-particle probability distribution function $P(z,\cos\beta)$, where z is the distance of the center of mass of the molecule from the silica surface.

$$P(z,\cos\beta) = \langle \delta(z - z_i)\delta(\cos\beta - \hat{\mathbf{u}}_i \cdot \hat{\mathbf{z}}) \rangle, \tag{2}$$

We examine in turn the effects of the various surfaces on $P(z,\cos\beta)$. The 5CB film deposited on top of the cristobalite (001) surface is characterized by two distinct interfaces: the bottom one, where the LC interacts with the crystal surface, and the top interface where the LC is exposed to vacuum. At the interface with vacuum the probability distribution function, shown in Figure 5, is characterized by a bilayer of molecules for both the isotropic and the nematic phases, as also found in the simulations of Ref. 19 and

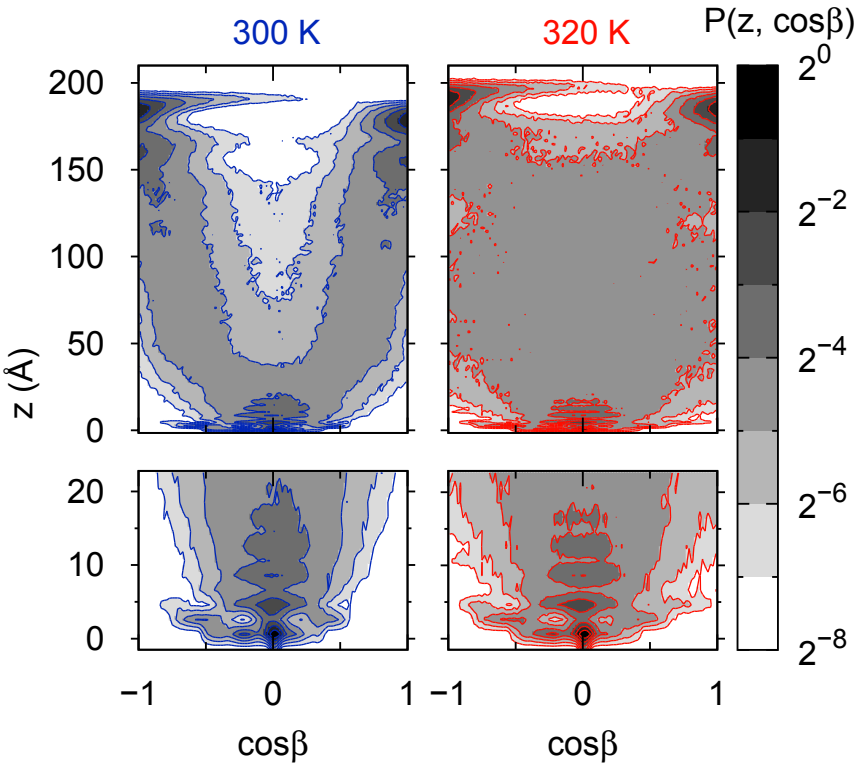

Figure 5: Gray-shaded contour map of the probability distribution function $P(z, \cos\beta)$ for 5CB on cristobalite (001) surface at 300 K (left panel) and 320 K (right panel). The bottom panels show a close-up of the function $P(z, \cos\beta)$ at the silica/5CB interface.

experimentally in Ref. 23. The overlayer LC molecules, closely interacting with the cristobalite (001) surface, have instead a planar alignment shown by the intense peak around $\cos\beta \sim 0$. It can also be seen from Figure 1 that there is a preferred azimuthal direction along the facet diagonal, even if we are not specifically concerned with that here. A smaller peak with negative $\cos\beta$ value, corresponding to a fraction of 5CB molecules pointing their cyano groups toward the silica surface, is also present. The alignment induced by the cristobalite surface appears to propagate only up to $\sim$ 50 Å into the 5CB film. In the isotropic phase, the 5CB molecules are randomly oriented in the central region of the sample while in the nematic phase the effect of the vacuum interface causes the molecules to align parallel to the surface normal.

A different physical picture emerges for the film of 2000 5CB molecules deposited on top of the low roughness (*smooth*) amorphous glass. As shown in Figure 6, the molecules

of 5CB still tend to align more parallel than perpendicular to the silica surface, but with a rather broad distribution. Considering a region of 20 Å from the solid surface, roughly corresponding to a molecular length we have a broad peak centered at $\cos\beta = 0$, but with a spread of molecular tilt angles up to $\sim \pm 15^\circ$ from the surface, compared to the sharp one observed for the cristobalite surface and indicating a loss of orientational order, that we will quantify later on. Furthermore, in this region close to the surface, the distribution, both in the nematic phase and in the isotropic phase is slightly asymmetric and biased toward negative $\cos\beta$ values, showing weak polar order with the cyano pointing towards the surface. This can be compared with the results for 5CB anchoring on fused silica obtained from SHG studies of Shen and co-workers[10] where the tilt angle, assuming a sharp Gaussian spread of tilts with a width of a few degrees, was found to be $\sim 22^\circ$ from the surface. Thus we have a broad agreement with reference 10, but with a kind of uniform distribution inside the conical tilt region instead of a sharp angle. It is interesting to see that after the tilt in the first monolayer a planar orientation is recovered, as found in.[27] The planar alignment is then maintained well inside the sample of 5CB: in the nematic phase it counterbalances the alignment induced by the interface with vacuum at ~ 170 Å from the solid surface, *i.e.* nearly twice the persistence length for cristobalite.

The amorphous surface characterized by the largest roughness among the three surfaces studied in this work, has a more dramatic effect on the morphology of the 5CB interface. As shown in Figure 7, the probability distribution functions $P(z, \cos\beta)$ at the silica interface does not have a peak at $\cos\beta = 0$ any more but, rather, a fairly uniform distribution of angles in the range $0 \leqslant \beta \leqslant \pi$ is observed for both the isotropic and nematic samples. This morphology corresponds to a disordering effect induced by the silica surface. In the nematic phase, a planar orientation is established after the first layer of molecules and this configuration extends up to 170 Å into the LC film, analogously to what observed for the smooth surface (Figure 6).

It is useful to derive the first few moments in a Legendre polynomial expansion of

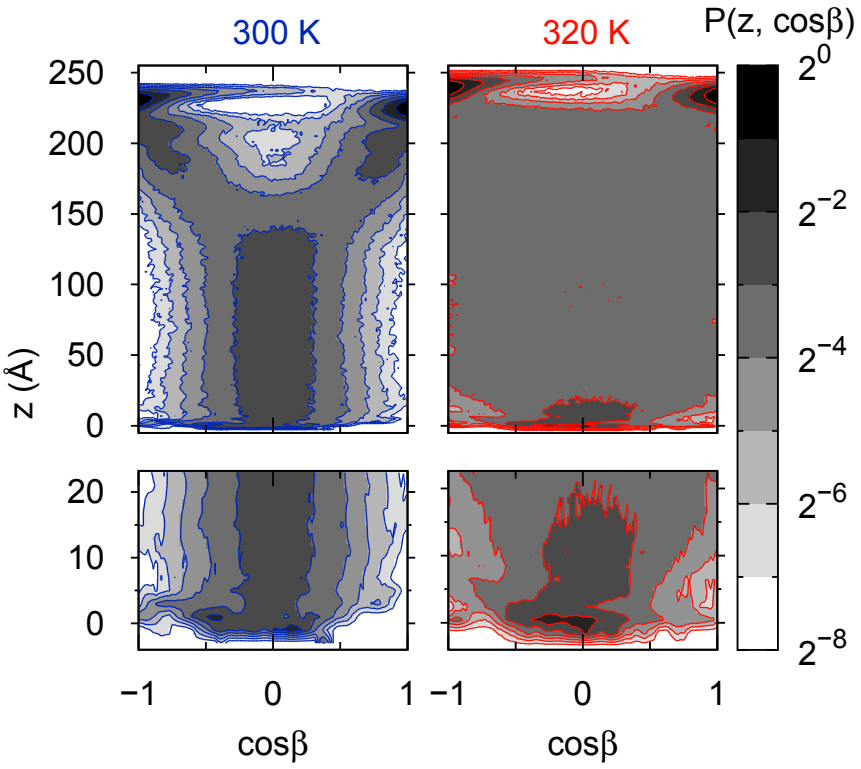

Figure 6: Gray-shaded contour map of the probability distribution function $P(z,\cos\beta)$ for 5CB on the smooth silica surface at 300 K (left panel) and 320 K (right panel). The bottom panels show a close-up of the function $P(z,\cos\beta)$ at the silica/5CB interface.

$P(z,\cos\beta)$, and in particular the density $\rho(z)$ and the polar and quadrupolar order parameters with respect to the surface normal z: $\langle P_1(z)\rangle \equiv \langle P_1(\cos\beta)\rangle_z$, $\langle P_2(z)\rangle \equiv \langle P_2(\cos\beta)\rangle_z$, calculated at a certain distance z from the solid surface, that we plot in Figure 8, Figure 9 and Figure 10.

$$P(z,\cos\beta) = \frac{\rho(z)}{\langle\rho\rangle}[\frac{1}{2} + \frac{3}{2}\langle P_1(\cos\beta)\rangle_z P_1(\cos\beta) + \frac{5}{2}\langle P_2(\cos\beta)\rangle_z P_2(\cos\beta) + ...] \qquad (3)$$

The density $\rho(z)$ of 5CB, uniform for the bulk nematic, shows significant fluctuations close to the two boundaries. At the interface with vacuum the density drops at the boundary, then the antiparallel arrangement of 5CB molecules, already observed in reference46, produces an oscillation of $\rho(z)$ corresponding to a couple of double-layers, as already seen in Figure 5, Figure 6, Figure 7. This feature which is present also to a weaker extent

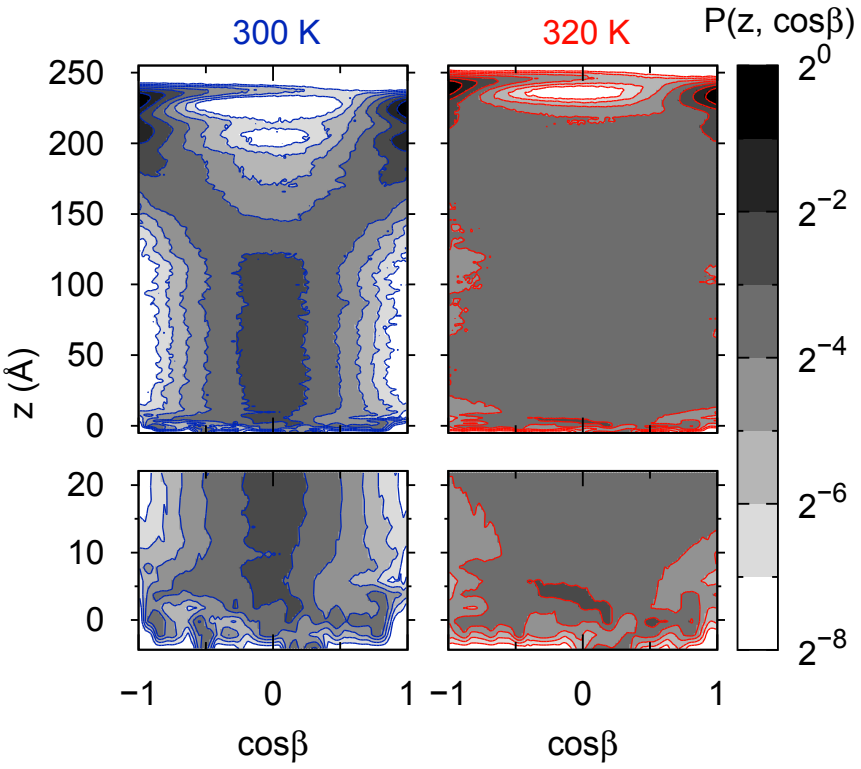

Figure 7: Gray-shaded contour map of the probability distribution function $P(z,\cos\beta)$ for 5CB on the rough silica surface at 300 K (left panel) and 320 K (right panel). The bottom panels show a close-up of the function $P(z,\cos\beta)$ at the silica/5CB interface.

in the isotropic phase is common to all films, irrespective of the solid surface. In all cases, no significant variation of the density is instead observed in the center of 5CB film. At the silica interface, a sharp peak and damped oscillations of the density are observed for the cristobalite. The peaks correspond to few successive planar layers of 5CB molecules coming in close contact with the atomically flat crystal surface. This is reminiscent of what we have already observed for 5CB on hydrogen terminated crystalline silicon[46] and also of what has been observed experimentally for other hybrid films by Musevic and collaborators using AFM.[54]

In order to compare the three 5CB samples, we have aligned the first peak of the density at $z = 0$, which thus indicates the 5CB/support interface. In the region with $z < 0$, represented as a gray-shaded area in Figure 8, the density goes abruptly to zero above the cristobalite surface, while it decreases smoothly above the glassy surfaces.

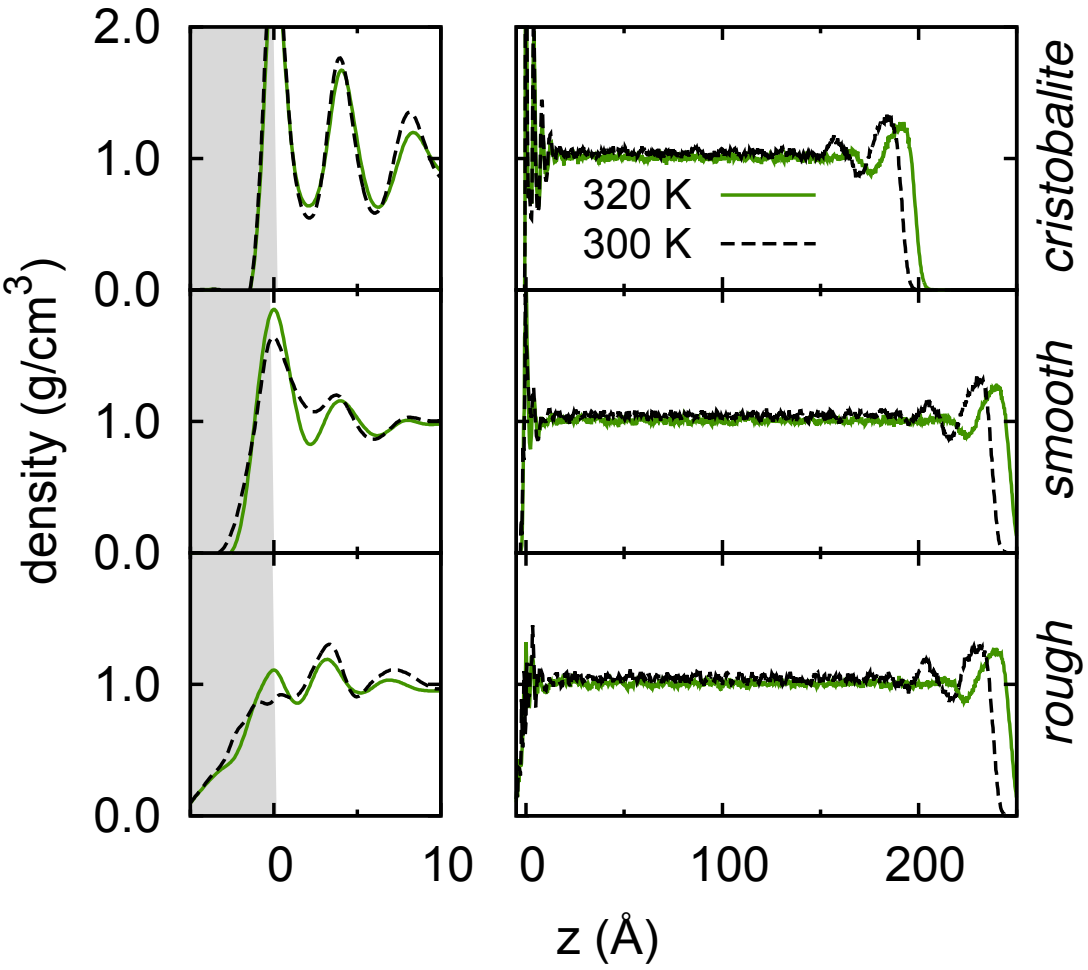

Figure 8: Density $\rho(z)$ of different 5CB films at T=300 K and 320 K across the film (right panel) and close to the silica (left panel), computed with respect to the normal at the surface, z. The 5CB/silica interface is chosen as the first peak of $\rho(z)$ and shifted at $z = 0$.

The polar order parameter $\langle P_1(z) \rangle$, computed with respect to the normal to the surface z (green curve in Figure 9) also provides evidence for the molecular organization of molecules in the different samples. At the interface with vacuum $\langle P_1(z) \rangle$ is negative, corresponding to the fact that the alkyl tails of 5CB molecules point toward the outside,[23] and then shows small oscillations corresponding to the formation of the polar layers of molecules oriented anti-parallel to each other already mentioned and experimentally observed by X-ray diffraction also in the bulk.[55]

A weak polar ordering is also observed in the proximity of the solid surface, both

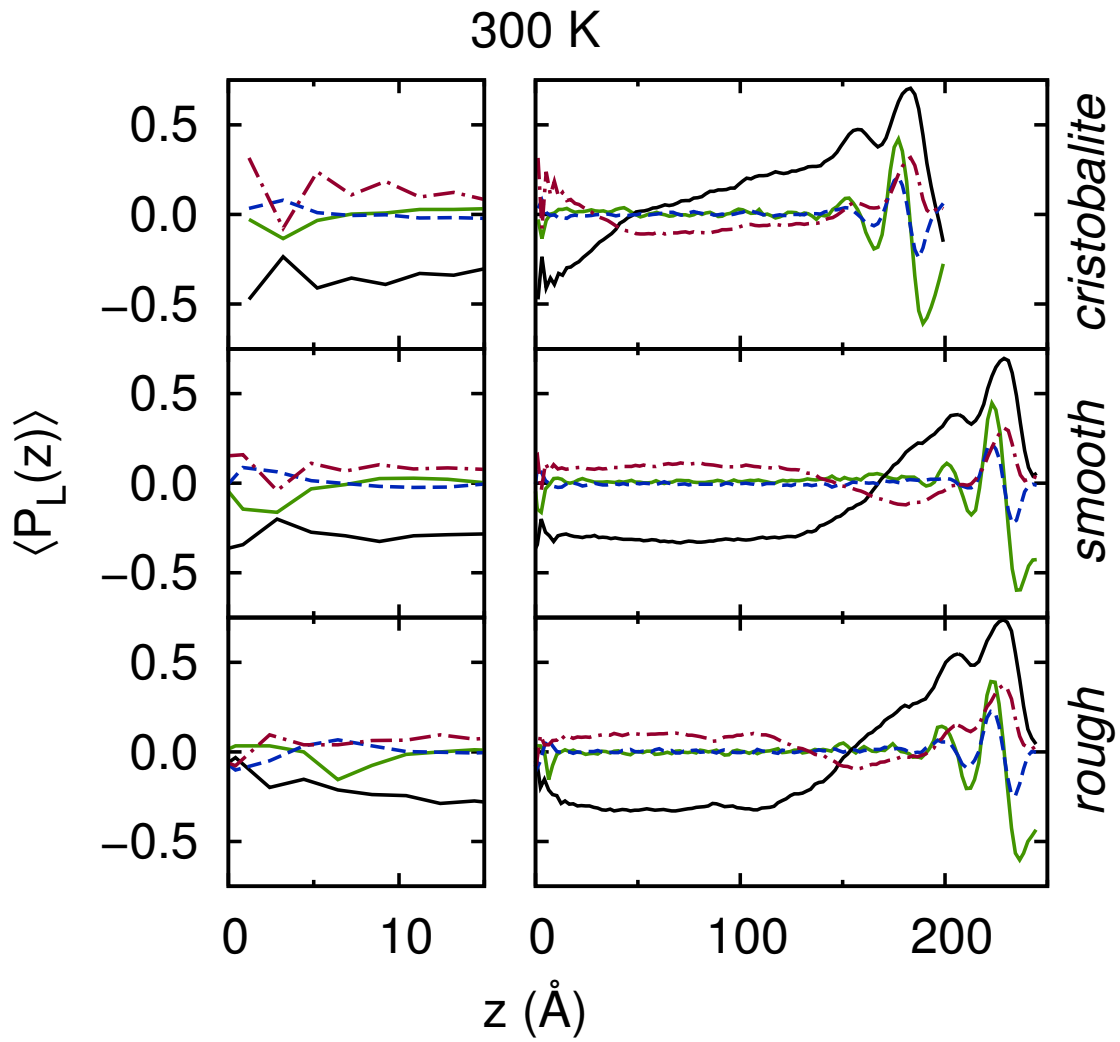

Figure 9: Order parameters $\langle P_1(z)\rangle$ (green line), $\langle P_2(z)\rangle$ (black line), $\langle P_3(z)\rangle$ (blue dashed line), $\langle P_4(z)\rangle$ (red dot-dashed line) of different 5CB films at T=300 K across the film (right panel) and close to the silica (left panel), computed with respect to the normal at the surface, z.

in the nematic and in the isotropic phases. The negative sign of $\langle P_1(z)\rangle$ at around 5 Å above the 5CB/support interface indicates a prevalence of 5CB molecules pointing their CN groups toward the silica.

The asymmetry induced by the surface causes a non zero value also of the third rank order parameter $\langle P_3(z)\rangle$ (blue dashed line) that determines the average non linear susceptibility tensor element χ^2_{zzz}, which in turn corresponds to a SHG observable.[10,56] We see that $\langle P_3(z)\rangle$ is different from zero only in a very thin region close to the surface.

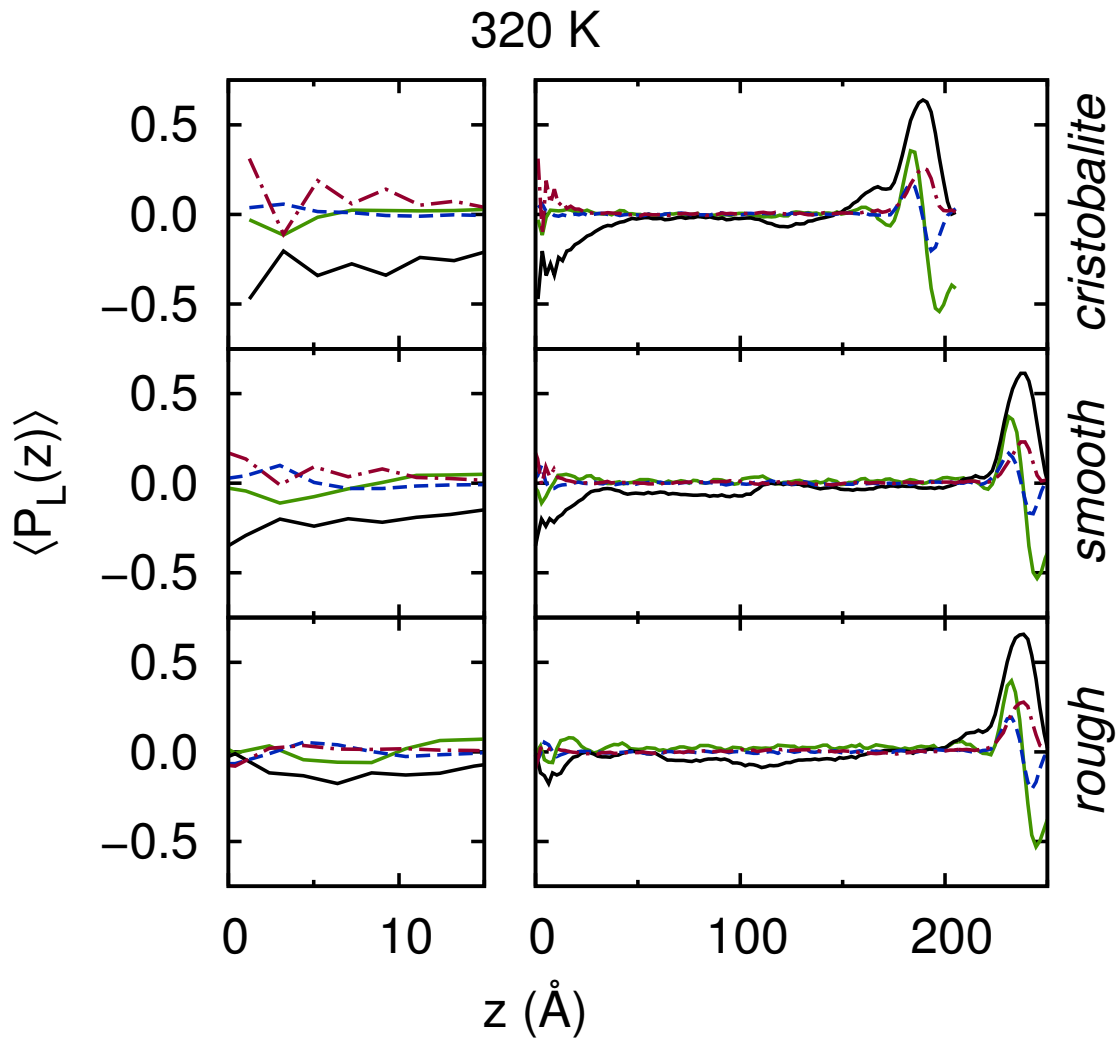

Figure 10: Order parameters $\langle P_1(z)\rangle$ (green line), $\langle P_2(z)\rangle$ (black line), $\langle P_3(z)\rangle$ (blue dashed line), $\langle P_4(z)\rangle$ (red dot-dashed line) of different 5CB films at T=320 K across the film (right panel) and close to the solid surface (left panel), computed with respect to the normal at the surface, z.

In Figure 9, Figure 10 we also report the fourth rank order parameter $\langle P_4(z)\rangle$ that can in principle be determined by depolarized Raman[57] or fluorescence depolarization[58] experiments. Although these are not available now, we hope our calculations will stimulate specific experiments.

An important, complementary, information can be obtained from the scalar order parameter $\langle P_2\rangle$, which expresses the ordering with respect to the local director $\mathbf{n}(z)$, wherever it might be oriented, rather than with respect to the fixed direction in space $\mathbf{z}$. $\langle P_2\rangle$

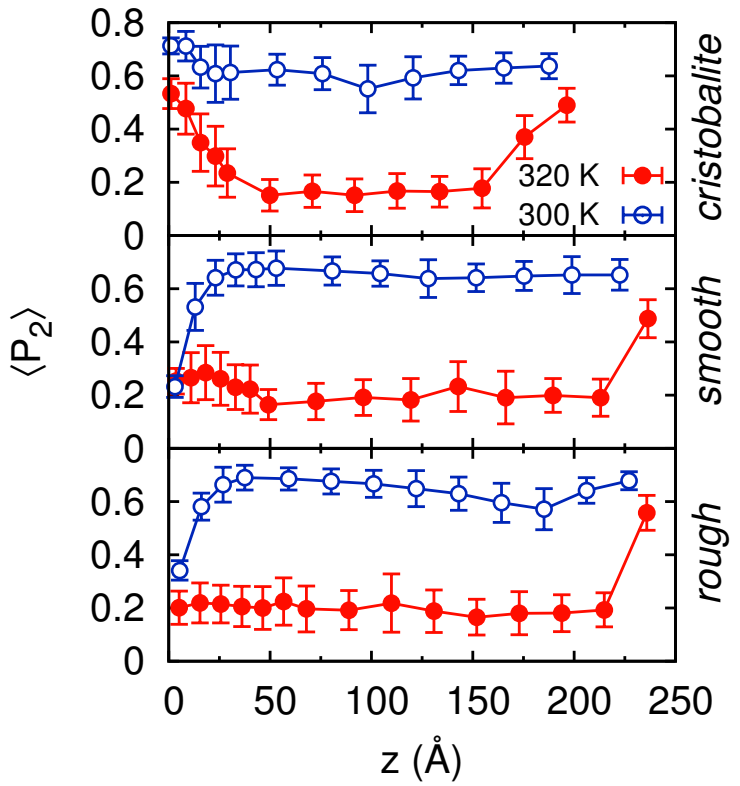

Figure 11: Scalar order parameter $\langle P_2 \rangle$ with eror bars of different 5CB films at T = 300 K (open symbols) and T = 320 K (full symbols) computed in different layers along the laboratory axis z.

and $\mathbf{n}(z)$ are obtained, as now well established, from the largest eigenvalue of the ordering matrix $\mathbf{Q}(z)$ and its corresponding eigenvector,[19,46] computed in layers parallel to the surface, as shown in Figure 11.

$$\mathbf{Q}(z) = < \sum_{i=1}^{N_L(t)} [3\hat{\mathbf{u}}_i(t) \otimes \hat{\mathbf{u}}_i(t) - \mathbf{I}]/2N_L(t) >_t, i \in L \tag{4}$$

where $\hat{\mathbf{u}}_i(t)$ is the chosen molecular axis, here, as we already mentioned, the principal axis of inertia. $\mathbf{I}$ is the identity matrix and the sum runs over all the N_L molecules present in the layer L centered at z at time t, while $< .. >_t$ is a time average over the MD equilibrated trajectories. This analysis clearly reveals up to which extent each interface influences the orientational ordering across the 5CB films. We have already seen from the probability distribution function $P(z, \cos\beta)$ that the interface with the vacuum (which is located at

$z \sim 200$ Å) induces the formation of a double-layer of highly-oriented molecules. Correspondingly, the order parameter computed in that region shows an increase of the $\langle P_2 \rangle$ value with respect to the central "bulk-like" region of the film. The ordering effect of the surface is more pronounced in the isotropic phase, where the value of $\langle P_2 \rangle$ at the vacuum interface is almost the same of that in the nematic phase, while in the center of 5CB film it drops to ~ 0.2. Similarly, the interface with cristobalite induces a strong ordering in the 5CB over-layer and, consequently, the value of $\langle P_2 \rangle$ increases with respect to the bulk of the sample. If we recall that the 5CB molecules at the cristobalite interface are preferentially oriented along the [110] direction of the facet, as shown in Figure 1, we see that this morphology is consistent with the empirically based expectations for a solid surface with planar non degenerate anchoring.[14] This surface order seems to be only weakly dependent on temperature, being similar both for the nematic and the isotropic temperatures studied. Local induced nematic order in the isotropic phase has also been found experimentally for another planar non degenerate aligning surface (rubbed polyimide),[59] although a longer tail of the scalar order was found in that case. Altogether the results we have found for 5CB on cristobalite [001] are similar to what we have found for 5CB on hydrogen terminated [001] silicon, hinting that they can be common to other planar homogeneous substrates as suggested in ref. 14.

However, the silica glass surfaces have a completely opposite effect on the 5CB sample and for both surfaces the value of $\langle P_2 \rangle$ decreases at the silica interface, rather than increasing. In general this corresponds to the empirical wisdom for support surfaces that are isotropic in the xy plane (planar degenerate),[14] but we can now analyze the phenomenon at molecular level. In particular, the decrease of the ordering parameter seems to be due to the amorphous and to some extent irregular nature of these surfaces, which favors different local orientations of 5CB molecules, as observed from the probability distribution functions shown in Figure 6 and Figure 7. The broad distribution of orientations has a disruptive effect on the scalar nematic order of 5CB, but in all cases this effect is limited

to the first few nanometers above the silica surface. After this region the 5CB molecules recover a bulk-like value of $\langle P_2 \rangle$, similar to that measured for the cristobalite sample. The decrease of order observed with increasing roughness is in agreement with theoretical predictions made by Barbero and Durand[60] and with experimental observations on SiO.[61]

While we have discussed until now the alignment of the molecular axis with respect to the normal and the scalar order, we have not yet examined how the director changes in this hybrid film[62–66] on going from the solid surface plane to the vacuum interface. It is worth noticing first that diagonalization of the $\mathbf{Q}$ matrix always produces an order parameter as its largest eigenvalue and thus formally a director as its associated eigenvector, even for an isotropic liquid. However, that eigenvector can be legitimately considered a director only if the phase is ordered, *i.e.* if $\langle P_2 \rangle$ is larger than the effective isotropic value. Given the fact that $\langle P_2 \rangle$ is intrinsically positive since $Tr\mathbf{Q} = 0$ and that the statistical error is at least of the order of ${N_L}^{\frac{1}{2}}$ if the number of molecules in a layer is N_L , we plot in Figure 12 the in-plane (*i.e.* , n_{xy}) and out-of-plane (*i.e.* , n_z) components of the molecular director $\mathbf{n}$ across the 5CB films[19] for the nematic phase only, with the additional limit to the cases where $\langle P_2 \rangle \lessapprox 0.3$, *i.e.* our chosen noise level for the orientational order in a layer (see also Figures 6, 7).

The film of 5CB shows a homeotropic alignment at the vacuum interface for all the samples studied, for both the isotropic and nematic phases: here, the n_z component has a value close to one while the n_{xy} component is close to zero. Conversely, the LC molecules close to the 5CB/support interface orient parallel to the surface, as can be seen from the high value of the n_{xy} component. The effect of the surface on the preferred alignment direction is maintained well after the effect on the value of the scalar order (cf. Figure 11) is ceased. This is in line with the expectation that the director orientation established at the aligning surface propagates for micron size correlation length. Here we have a propagation of some nanometers into the sample, after which we observe a switching to the

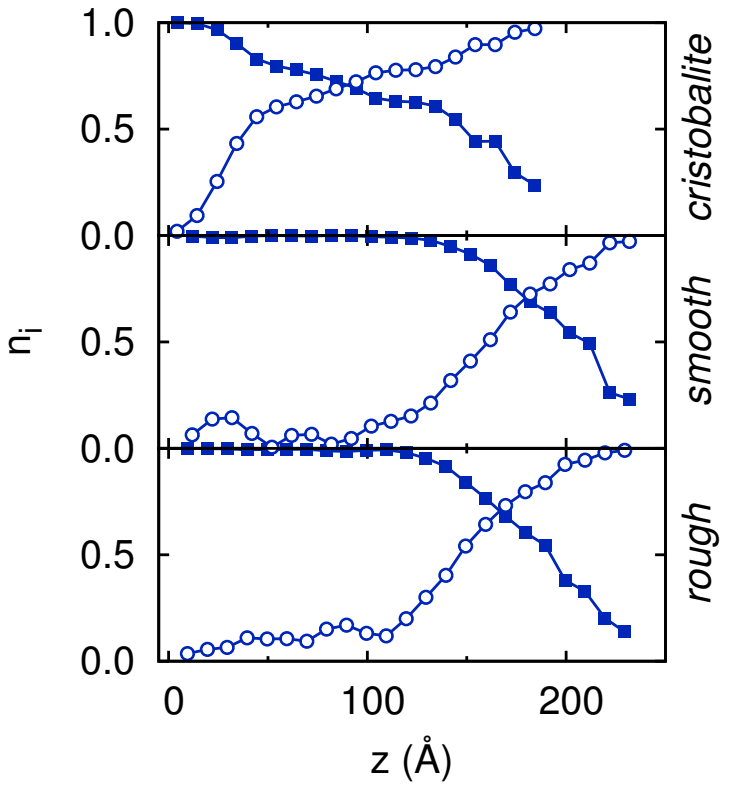

Figure 12: Director components $n_{xy} = \sqrt{n_x^2 + n_y^2}$ (solid symbols) and n_z (open symbols) for 5CB samples on the three surfaces computed at T=300 K for different layers along the laboratory axis z.

quasi-homeotropic alignment induced by the free surface. For the cristobalite case, Figure 12 shows that the parallel alignment of the director induced by the surface propagates up to ~ 90 Å above the surface before the ordering effect induced by the antagonistic anchoring imposed by the vacuum interface takes over and the alignment turns homeotropic.

We have seen that silica glass surfaces lower the local scalar order parameter for the nematic phase at contact distance. On the hand, after the first few layers the director become well defined and parallel to the surface and this effect extends well into the sample: for both amorphous surfaces, the region where LC molecules lye in a planar configuration ends at about 170 Å above the surface.

From these results it can be concluded that the morphology of the silica surface has a dramatic effect on the properties of the overlying film of LC molecules. The first effect is

on the scalar order that is increased or decreased for the first few layers. The second is the director orientation and its propagation. A crystalline and well-ordered surface like that of cristobalite has an effect that is relatively local on the director orientation, while an amorphous surface has an effect on the director correlation length which extends far into the 5CB sample.

Calculation of the *mean field* anchoring strength

A key quantity for the study of surface interactions with thin films is the anchoring strength $W_2^A(z)$ which rules, alongside with the film thickness,[67] phenomena such as thickness–dependent[14,68] and temperature–dependent[69] anchoring transitions, and determines the voltage required for switching the alignment of LC films and the relaxation time required to return to equilibrium after the field is removed. Although the simulation of these transitions is beyond the scope of this study and probably still too demanding for atomistic simulations, we have here the possibility of measuring the energy which anchors each LC molecule and its surface-induced variation.[19]

We calculated the free energy as a function of molecular orientation $\cos\beta$ and the distance z_i from the SiO_2 surfaces from the Boltzmann inversion of the corresponding positional–orientational distribution functions $P(z,\cos\beta)$, obtained as a histogram from the simulated trajectory:

$$W(z_i,\cos\beta) = -k_B T \ln P(z_i,\cos\beta) N(z_i) / A \tag{5}$$

where the subscript i indicates that z_i is a discrete variable, and $P(z_i,\cos\beta)$ is normalized to one for each layer z_i, here of width 10 Å.

We then fitted this effective potential energy $W(z_i,\cos\beta)$ with a Rapini-Papoular expression (cf. equation 1). Employing this formula implies the assumption of the free energy $W(z_i,\cos\beta)$ to be a parabola centered in $\beta_{eq}^d(z_i)$: we verified that this holds true

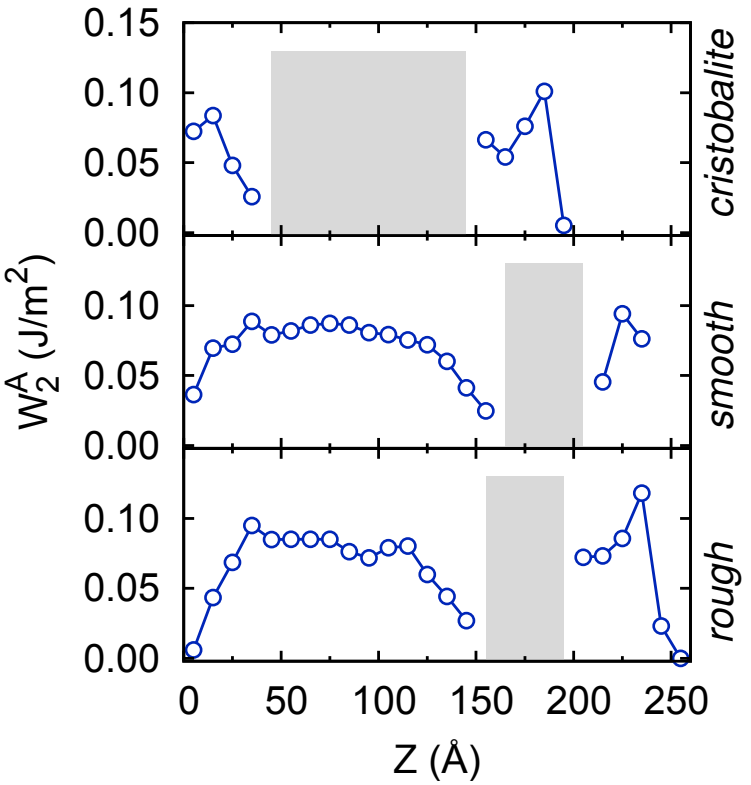

Figure 13: Rapini-like anchoring coefficient W_2^A for 5CB as a function of distance from the cristobalite, smooth and rough silica surfaces at 300 K. The coefficients are calculated for sections of the sample with a thickness of 10 Å. Anchoring coefficients are not calculated in the inner regions corresponding to a switch over between the two antagonistic surfaces (grey areas).

for all the 5CB layers but in the close proximity to the interfaces, where also polar terms come into play in particular for vacuum, as demonstrated by the non negligible values of $\langle P_1(z) \rangle$ previously discussed.

The anchoring coefficients as a function of the distance from the surface were then obtained by minimizing the following weighted square error sum with respect to the parameters $W_0^A(z)$ and $W_2^A(z)$:

$$\chi^2(z_i) = \sum_{\cos\beta} P(z_i, \cos\beta) \left\{ W(z_i, \cos\beta) - W_0^A(z_i) + \frac{1}{2} W_2^A(z_i) \sin^2[\beta - \beta_{eq}^d(z_i)] \right\}^2 \quad (6)$$

where β is the angle between a molecule and the normal to the surface and $\beta^d_{eq}(z_i)$ is the local orientation of the $i-th$ layer phase director. For simplicity, we used $\beta^d_{eq}(z_i) = 0$ when $n_z < \cos(\pi/6)$, $\beta^d_{eq}(z) = \pi/2$ when $n_z > \cos(\pi/3)$, and we did not perform the fit in the switching region, defined as $\cos(\pi/6) < n_z < \cos(\pi/3)$ (the director component normal to the surface n_z is shown in Figure 12).

The calculated $W_2^A(z_i)$ coefficients in the nematic phase are shown in Figure 13 for all the samples studied. These values measure how strong is the orienting mean field exerted by the 5CB molecules on one probe LC molecule in each layer.

Going into the details of the different interfaces, vacuum seems to strongly anchor 5CB molecules in a range of about 25 Å, corresponding to the length of the 5CB double layer "dimer"[68] which forms at this interface. Among the surfaces studied, cristobalite has the larger anchoring coefficients, but also the shorter range of action. Amorphous silica surfaces yield to lower $W_2^A(z_i)$ values with respect to cristobalite, but their range of effect is longer and clearly correlated with the extent of the region of planar alignment. Also differently from cristobalite, the highest measured coefficients for amorphous surfaces are found at $z \sim$ 50–100 Å, while around $z = 0$ the 5CB order parameter is quite low and consequently the free energy profile is rather flat.

Consistently with our previous study of 5CB films on a Si (001):H surface,[19] the anchoring strengths measured from simulation are much larger than the ones reported in the literature for thick films of cyanobiphenyls via electro-optical measurements on several substrates (10-100 mJ/m^2 vs 0.01-1 mJ/m^2).[67,70–72]

Larger values, comparable to our ones, have been instead measured by recent surface force experiments on nanometric hybrid films.[68] This variance can be ascribed to several factors. The foremost is probably the strong dependence of the anchoring coefficients on the distance from the surface. Thus experimental techniques probing different regions away from a surface can provide different results, consistently with the wide spread of values reported in the literature. Here we are looking at nanosize effects and the an-

choring strength is known to increase with decreasing film thickness.[67] Other factors can be invoked, as the inadequacy of Rapini-Papoular expression in describing the free energy profile for large deviations from the equilibrium value $\beta^d_{eq}(z_i)$ which are probed by electro-optical switching experiments, the difficulty in disentangling anchoring and adhesion forces in AFM measurements, and the possibility that LC molecules very close to the surface do not directly contribute to the anchoring because they are trapped by adhesion forces and surface roughness.[73]

In any case it seems clear from our study that roughness, even at the nanoscale can deeply change the anchoring characteristic of the surface with a given chemical composition.

Conclusions

In this work we have studied in detail the molecular organization of three thin films, of thickness $\sim$ 20 nm , of the liquid crystal 5CB on crystalline and amorphous silica with the help of atomistic MD simulations. A united-atom force field,[46] which was previously optimized to reproduce the nematic-isotropic transition temperatures of several members of the *n*CB LC family, has been used to describe the LC phase. A procedure for generating crystalline and amorphous silica slabs with controlled surface roughness that should be of rather general use has been proposed.

We find that the crystalline surface ((001) facet of cristobalite) induces a strong planar homogeneous alignment and an increase of the scalar order parameter of 5CB at the surface decaying, in the nematic, in $\sim$ 30 Å from the solid interface. The planar alignment of the director persists instead for $\sim$ 100 Å before turning into the perpendicular orientation imposed by the free boundary. For the amorphous silica surfaces, we observe the inducement of local disorder to nearly isotropic values, but with some polar order for the first couple of nm, where a preference for CN orientation toward the surface is found. After

this the bulk order is recovered in the nematic, and a planar orientation for the director established, reminiscent of what was found experimentally in.[26,27] The planar orientation induced by these amorphous surfaces is however much longer ranged than that of cristobalite, and extends up to $\sim$ 170 Å above the glass interface. As for anchoring energies, we have determined the generalized Rapini-Papoular coefficients at different distances from the surfaces. For cristobalite we have found, as in our previous work on the 5CB-hydrogen terminated crystalline silicon interface,[19] very strong values, of the order of 100 mJ/m^2, for the first layers. These large values are compatible with those obtained by very recent surface force experiments on a mica-5CB-CTAB hybrid film.[68] In the case of amorphous silica, we find that the Rapini anchoring coefficient is only smaller than that of cristobalite at the surface, where is further lowered by increasing the surface roughness but the anchoring is stronger and more persistent at larger distances[59] than that for the crystalline substrate.

In summary we have performed the first predictive simulations of a nematic on a glassy and crystalline silica surface, clarifying the role of surface crystallinity and roughness on alignment and anchoring, important phenomena described only empirically or at a continuum level, difficult to justify at the nanoscale, until now. The combination of atomistic simulations and experiments on surfaces with controlled nano-roughness promises to be an important area of development to improve our understanding of anchoring in liquid crystals.

Acknowledgement

We acknowledge the European Project MINOTOR (Grant No. FP7-NMP-228424) and MIUR PRIN national project "Novel ordered systems for high response molecular devices" for funding this research and CINECA Supercomputing Center for providing computer time through a ISCRA grant.

References

(1) Chigrinov, V. G. *Liquid Crystal Devices. Physics and Applications*; Artech House, 1999.

(2) Semenza, P. *Nat. Photonics* **2007**, *1*, 267–268.

(3) Beljonne, D.; Cornil, J.; Muccioli, L.; Zannoni, C.; Brédas, J.-L.; Castet, F. *Chem. Mater.* **2011**, *23*, 591–609.

(4) Vilan, A.; Yaffe, O.; Biller, A.; Salomon, A.; Kahn, A.; Cahen, D. *Adv. Mater.* **2010**, *22*, 140–159.

(5) Israelachvili, J. *Intermolecular and Surface Forces*; Academic Press, 1992.

(6) Blinov, L. M.; Chigrinov, V. G. *Electrooptic effects in liquid crystal materials*; Springer-Verlag, 1994.

(7) Voitchovsky, K.; Kuna, J.; Contera, S.; Tosatti, E.; Stellacci, F. *Nature Nanotech.* **2010**, *5*, 401–405.

(8) Yokoyama, H. *Mol. Cryst. Liq. Cryst.* **1988**, *165*, 265–316.

(9) Jérôme, B. *Rep. Progr. Phys.* **1991**, *54*, 391–451.

(10) Zhuang, X.; Marrucci, L.; Johannsmann, D.; Shen, Y. *Mol. Cryst. Liq. Cryst. A* **1995**, *262*, 1323–1331.

(11) Rasing, T.; Muševič, I. *Surfaces And Interfaces Of Liquid Crystals*; Springer, 2004.

(12) Barbero, G.; Evangelista, L. R. *Adsorption Phenomena and Anchoring Energy in Nematic Liquid Crystals*; Taylor & Francis, 2006.

(13) Hoogboom, J.; Elemans, J.; Rasing, T.; Rowan, A.; Nolte, R. *Polym. Internat.* **2007**, *56*, 1186–1191.

(14) Cazabat, A.; Delabre, U.; Richard, C.; Sang, Y. *Adv. Colloids Interf. Sci.* **2011**, *168*, 29–39.

(15) Rapini, A.; Papoular, M. *J. Phys. Colloq.* **1969**, *40*, C3–490.

(16) de Gennes, P. G. *The Physics of Liquid Crystals*; International Series of Monographs on Physics; Clarendon Press: Oxford, 1974.

(17) Teixeira, P. I. C.; Sluckin, T. J. *J. Chem. Phys.* **1992**, *97*, 1498–1509.

(18) Fukuda, J.; Yoneya, M.; Yokoyama, H. *Phys. Rev. Lett.* **2007**, *98*, 187803.

(19) Pizzirusso, A.; Berardi, R.; Muccioli, L.; Ricci, M.; Zannoni, C. *Chem. Sci.* **2012**, *3*, 573–579.

(20) Janning, J. *Appl. Phys. Lett.* **1972**, *21*, 173–174.

(21) Urbach, W.; Boix, M.; Guyon, E. *Appl. Phys. Lett.* **1974**, *25*, 479–481.

(22) Armitage, D. *J. Appl. Phys.* **1980**, *51*, 2552–2555.

(23) Valignat, M. P.; Villette, S.; Li, J.; Barberi, R.; Bartolino, R.; Dubois-Violette, E.; Cazabat, A. M. *Phys. Rev. Lett.* **1996**, *77*, 1994–1997.

(24) Berreman, D. W. *Phys. Rev. Lett.* **1972**, *28*, 1683–1686.

(25) Sprokel, G. *Mol. Cryst. Liq. Cryst.* **1977**, *42*, 233–243.

(26) Chen, C.; Bos, P.; Anderson, J. *Liq. Cryst.* **2008**, *35*, 465–481.

(27) Reznikov, Y.; Ostroverkhova, O.; Singer, K.; Kim, J.; Kumar, S.; Lavrentovich, O.; Wang, B.; West, J. *Phys. Rev. Lett.* **2000**, *84*, 1930–1933.

(28) Reznikov, Y.; Ostroverkhova, O.; Singer, K.; Kim, J.; Kumar, S.; Lavrentovich, O.; Wang, B.; West, J. *Phys. Rev. Lett.* **2001**, *87*, 249602, rebuttal of Park Takezoe criticism.

(29) Park, B.; Wu, J. W.; Takezoe, H. *Phys. Rev. Lett.* **2001**, *87*, 249601.

(30) Barth, T. F. W. *Am. J. Sci.* **1932**, *23*, 350–356.

(31) Gale, J.; Rohl, A. *Mol. Simul.* **2003**, *29*, 291–341.

(32) The General Utility Lattice Program (GULP). https://projects.ivec.org/gulp.

(33) Du, J.; Cormack, A. N. *J. Am. Chem. Soc.* **2005**, *88*, 2532–2539.

(34) Jerome, B.; Pieranski, P. *Europhys. Lett.* **1990**, *13*, 55–59.

(35) Della Valle, R. G.; Andersen, H. C. *J. Chem. Phys.* **1992**, *97*, 2682–2689.

(36) Plimpton, S. *J. Comp. Phys.* **1995**, *117*, 1–19.

(37) LAMMPS Molecular Dynamics Simulator. http://lammps.sandia.gov.

(38) Mozzi, R. L.; Warren, B. E. *J. Appl. Crystallogr.* **1969**, *2*, 164–172.

(39) Voss, N.; Gerstein, M.; Steitz, T.; Moore, P. *J. Mol. Biol.* **2006**, *360*, 893–906.

(40) V: Voss Volume Voxelator^3. http://geometry.molmovdb.org/3v/ .

(41) Guha, R.; Howard, M. T.; Hutchison, G. R.; Murray-Rust, P.; Rzepa, H.; Steinbeck, C.; Wegner, J.; Willighagen, E. L. *J. Chem. Inf. Model.* **2006**, *46*, 991–998.

(42) The Open Babel Package, version 2.0.1. httpopenbabel.sourceforge.net.

(43) Mantina, M.; Chamberlin, A. C.; Valero, R.; Cramer, C. J.; Truhlar, D. G. *J. Phys. Chem. A* **2009**, *113*, 5806–5812.

(44) Bondi, A. *J. Phys. Chem.* **1964**, *68*, 441–451.

(45) Mate, C. M. *Tribology on the Small Scale A Bottom Up Approach to Friction, Lubrication, and Wear*; Oxford University Press, 2007.

(46) Tiberio, G.; Muccioli, L.; Berardi, R.; Zannoni, C. *Chem. Phys. Chem.* **2009**, *10*, 125–136.

(47) Al-Matar, A. K.; Rockstraw, D. A. *J. Comput. Chem.* **2004**, *25*, 660–668.

(48) Cruz-Chu, E. R.; Aksimentiev, A.; Schulten, K. *J. Phys. Chem. B* **2006**, *110*, 21497–21508.

(49) Phillips, J. C.; Braun, R.; Wang, W.; Gumbart, J.; Tajkhorshid, E.; Villa, E.; Chipot, C.; Skeel, R. D.; Kalé, L.; Schulten, K. *J. Comput. Chem.* **2005**, *26*, 1781–1802.

(50) Parry, D. E. *Surf. Sci.* **1975**, *49*, 433–440.

(51) Parry, D. E. *Surf. Sci.* **1976**, *54*, 195.

(52) Ye, I.-C.; Berkowitz, M. *J. Chem. Phys* **1999**, *111*, 3155–3162.

(53) Smith, E. R. *Proc. R. Soc. London A* **1982**, *381*, 241–247.

(54) Carbone, G.; Lombardo, G.; Barberi, R.; Muševič, I.; Tkalec, U. *Phys. Rev. Lett.* **2009**, *103*, 167801.

(55) Leadbetter, A.; Richardson, R.; Colling, C. *J. Phys. C1* **1975**, *36*, 37–43.

(56) Jérôme, B.; Shen, Y. R. *Phys. Rev. E* **1993**, *48*, 4556–4574.

(57) Sanchez-Castillo, A.; Osipov, M.; Giesselmann, F. *Phys. Rev. E* **2010**, *81*, 02170.

(58) Zannoni, C. *Mol. Phys.* **1979**, *38*, 1813–1827.

(59) Lee, J. H.; Atherton, T. J.; Barna, V.; De Luca, A.; Bruno, E.; Petschek, R. G.; Rosenblatt, C. *Phys. Rev. Lett.* **2009**, *102*, 167801.

(60) Barbero, G.; Durand, G. *J. Phys. II France* **1991**, *1*, 651–658.

(61) Monkade, M.; Martinot-Lagarde, P.; Durand, G.; Granjean, C. . *J. Phys. II France* **1997**, *7*, 1577–1596.

(62) Palffy-Muhoray, P.; Gartland, E. C.; Kelly, J. R. *Liq. Cryst.* **1994**, *16*, 713–718.

(63) West, J.; Magyar, G.; Kelly,; Kobayashi, S.; Iimura, Y.; Yoshida, *Appl. Phys. Lett.* **1995**, *67*, 155–157.

(64) Chiccoli, C.; Lavrentovich, O.; Pasini, P.; Zannoni, C. *Phys. Rev. Lett.* **1997**, *79*, 4401–4404.

(65) Barbero, G.; Barberi, R. *J. de Physique* **1983**, *44*, 609–616.

(66) Chiccoli, C.; Pasini, P.; Sarlah, A.; Zannoni, C.; Zumer, S. *Phys. Rev. E* **2003**, *67*, 050703.

(67) Luckhurst, G.; Miyamoto, T.; Sugimura, A.; Takashiro, T.; Timimi, B. *J. Chem. Phys.* **2001**, *114*, 10493–10503.

(68) Ruths, M.; Zappone, B. *Langmuir* **2012**, *28*, 8371–8383.

(69) Castellon, E.; Zayat, M.; Levy, D. *Phys. Chem. Chem. Phys.* **2009**, *11*, 6234–6241.

(70) Blinov, L. M.; Kabayenkov, A. Y.; Sonin, A. A. *Liq. Cryst.* **1989**, *5*, 645–661.

(71) Wittebrood, M.; Luijendijk, D.; Stallinga, S.; Rasing, T.; Musevic, I. *Phys. Rev. E* **1996**, *54*, 5232–5234.

(72) Calus, S.; Rau, D.; Huber, P.; Kityk, A. *Phys. Rev. E* **2012**, *86*, 021701.

(73) Carbone, G.; Zappone, B.; Barberi, R.; Bartolino, R.; Musevic, I. *Phys. Rev. E* **2011**, *83*, 051707.